Structural and electrical properties of metastable defects in hydrogenated amorphous silicon

J. Melskens,[1,*] A. Schnegg,[2] A. Baldansuren,[2,†] K. Lips,[2,‡] M. P. Plokker,[3] S. W. H. Eijt,[3] H. Schut,[4] M. Fischer,[1] M. Zeman,[1] and A. H. M. Smets[1,§]

[1]*Photovoltaic Materials and Devices, Faculty of Electrical Engineering, Mathematics and Computer Science, Delft University of Technology, Mekelweg 4, 2628 CD, Delft, Netherlands*

[2]*Berlin Joint EPR lab, Institut für Silizium-Photovoltaik, Helmholtz-Zentrum Berlin für Materialen und Energie, Kekuléstrasse 5, 12489 Berlin, Germany*

[3]*Fundamental Aspects of Materials and Energy, Faculty of Applied Sciences, Delft University of Technology, Mekelweg 15, 2629 JB, Delft, Netherlands*

[4]*Neutron and Positron Methods in Materials, Faculty of Applied Sciences, Delft University of Technology, Mekelweg 15, 2629 JB, Delft, Netherlands*

(Received 1 December 2014; revised manuscript received 22 May 2015; published 11 June 2015)

The structural and electrical properties of metastable defects in various types of hydrogenated amorphous silicon have been studied using a powerful combination of continuous wave electron-paramagnetic resonance spectroscopy, electron spin echo (ESE) decay measurements, and Doppler broadening positron annihilation spectroscopy. The observed dependence of the paramagnetic defect density on the Doppler *S* parameter indicates that porous, nanosized void-rich materials exhibit higher spin densities, while dense, divacancy-dominated materials show smaller spin densities. However, after light soaking more similar spin densities are observed, indicating a long-term defect creation process in the Staebler-Wronski effect that does not depend on the a-Si:H nanostructure. From ESE decays it appears that there are fast and slowly relaxing defect types, which are linked to various defect configurations in small and large open volume deficiencies. A nanoscopic model for the creation of light-induced defects in the a-Si:H nanostructure is proposed.

DOI: 10.1103/PhysRevB.91.245207 PACS number(s): 73.61.Jc, 76.30.−v, 78.30.−j, 78.70.Bj

The light-induced degradation (LID) of hydrogenated amorphous silicon (a-Si:H), also known as the Staebler-Wronski effect (SWE) [1,2], has been extremely thoroughly investigated in the past decades [3–21]. Although the origin of the SWE and the nature of native and metastable defects is still poorly understood, impressive progress has been made in, for instance, the development of thin-film silicon (TF Si) solar cells. Record initial and stable conversion efficiencies of 16.3% [22] and 13.4%–13.6% [23,24], respectively, have been reported for small area ($\sim$1 cm^2) solar cells, all in triple-junction configuration. However, the amorphous junction produces most of the power in such solar cells, which means that fundamentally understanding the SWE is still important when aiming to increase the conversion efficiency of TF Si solar cells. Successfully applied LID-reduction methods include hydrogen (H_2) dilution of the silane gas (SiH_4) used during the plasma-enhanced chemical vapor deposition (PECVD) [25,26] and the use of a triode PECVD reactor [27,28]. However, the film growth follows such a complex interplay of deposition, etching, and hydrogen (H) effusion that the precise role of H in the a-Si:H nanostructure and the SWE remains obscured, although various growth models have been proposed [29].

Although H can reduce the (metastable) defect density in a-Si:H, it is unclear how the H passivation of dangling bonds (dbs) takes place exactly. This is due to the complexity of the a-Si:H nanostructure, which has proven to be a serious obstacle in accurately describing the defects in a-Si:H and the SWE-related recombination processes. Often, the nanostructure is modeled as a continuous random network where isolated dbs form the dominant defects [30]. Although the simplicity of the continuous random network is appealing, many experimental results have explicitly questioned its correctness as a description of the a-Si:H nanostructure [15,17,19,31,32]. Additionally, recent electron-paramagnetic resonance (EPR) studies indicate that isolated dbs are not the only defects in the nanostructure. Instead, at least two distinct types of defects are involved in the SWE [33,34]. This suggests that an alternative view on the nanostructure is needed, like the so-called disordered network with hydrogenated vacancies [35,36], also termed the anisotropic disordered network [31,32]. Note that the disordered network with hydrogenated vacancies consists of regions dominated by various types of open volume deficiencies, i.e., divacancies, multivacancies, and nanosized voids, which are embedded in disordered regions similar to the continuous random network. In view of these findings, the objective of this study is to gain insight into both the structural and electrical defect properties that govern the SWE.

In this work, we investigate four a-Si:H films deposited by radiofrequency (rf) PECVD on Corning XG glass, crystalline silicon (c-Si), and aluminum (Al) foil substrates. The deposition conditions for the films, as shown in Table I, are chosen such that the nanostructure and light-soaking stability of the different materials vary significantly. The gas flow rate ratio $R = [H_2]/[SiH_4]$ was varied such that two dense, high-quality types of a-Si:H could be deposited at low pressure, *p*. One film

*Present address: Department of Applied Physics, Eindhoven University of Technology, P.O. Box 513, 5600 MB Eindhoven, Netherlands; j.melskens@tue.nl

†Present address: The Photon Science Institute, EPSRC National EPR Facility and Service, School of Chemistry, The University of Manchester, Oxford Road, Manchester M13 9PL, United Kingdom.

‡lips@helmholtz-berlin.de

§a.h.m.smets@tudelft.nl

TABLE I. Deposition conditions and material properties for a-Si:H films with varying nanostructures. Note that the total atomic H content, c_H, the atomic H content in the Si-H high stretching mode, $c_{H,HSM}$, and the nanostructure parameter, R^*, are obtained by considering the Si-H wagging and stretching modes respectively, as determined by FTIR spectroscopy.

Sample description	P [mbar]	P_{rf} [W/cm^2]	ϕ_{H2} [SCCM][a]	ϕ_{SiH4} [SCCM]	T_s [°C]	r_d [nm/min]	c_H [at. %]	$c_{H,HSM}$ [at. %]	R^* [—]	S/S_{c-Si} [—]
Dense $R = 10$	2	0.024	200	20	180	6.25	8.8	0.18	0.02	1.019
Dense $R = 0$	0.7	0.024	0	40	180	11.1	8.1	0.24	0.03	1.030
High $pR = 50$	8	0.069	200	4	150	11.0	12.4	0.74	0.06	1.027
Porous $R = 0$	1	0.069	0	40	160	43.0	12.8	6.1	0.48	1.058

[a]SCCM denotes cubic centimeters per minute at STP.

was deposited from undiluted SiH_4 ($R = 0$) while another was deposited from moderately H_2-diluted SiH_4 ($R = 10$). These two films are investigated here because the latter is known to have a higher light-soaking stability, although the responsible nanostructural mechanism that can explain this difference is unknown [25,26]. Furthermore, a porous $R = 0$ film was deposited by increasing the rf power density, P_{rf}, which in turn increases the deposition rate, r_d. This a-Si:H material serves as an interesting reference, since it is known to have a poor light-soaking stability due to the presence of nanosized voids [37], which is indicated by a relatively large high stretching mode (HSM) intensity as indicated by Fourier transform infrared (FTIR) spectroscopy [31]. This film is indeed porous, while all others are dense, as illustrated in Table I by the much larger nanostructure parameter R^*, which is defined as the relative contribution of the HSM to the total infrared absorption induced by the Si-H stretching modes. Note that the films deposited on c-Si substrates were used to enable FTIR measurements in transmittance mode. Finally, we investigate another type of a-Si:H that is processed at high p from strongly H_2-diluted SiH_4 [16,38–41]. This kind of a-Si:H results in solar cells with a high open-circuit voltage when used as an absorber layer due to the increased band gap with respect to low-p a-Si:H. However, the nature of the native and metastable defects in high-p a-Si:H has not yet been studied.

To study the nature of the defects in the different a-Si:H nanostructures and pave the way towards SWE mitigation we employ a powerful combination of Doppler broadening positron annihilation spectroscopy (DBPAS) [31,32], quantitative continuous wave electron-paramagnetic resonance (cw-EPR) spectroscopy, and electron spin echo (ESE) decay measurements [34]. DBPAS is utilized to determine the dominant type of open volume deficiency in the material, as more valence electrons are probed by the implanted positron when the average open volume increases in size. Quantitative cw-EPR spectroscopy yields the total db density by counting the number of unpaired db spins per volume unit. Additionally, ESE decay measurements are employed to study the average defect distance and the formation of defect clusters, since the ESE decay of clustered and nonclustered dangling bonds is different. a-Si:H films on glass and Al foil were used for the DBPAS and EPR experiments, respectively. For the EPR experiments the 1-μm-thick films were removed from the substrates by wet etching (10% hydrochloric acid) after which the dried flakes were collected into quartz tubes. Note that one half of each Al foil sample was prepared in this way prior to light soaking and the other half only after light soaking. Light soaking was conducted for 400 h using an AM1.5 solar simulator at an ambient temperature of 50 °C. A red filter with a cutoff wavelength of 630 nm was used during light soaking to avoid inhomogeneous LID of the films [42]. A systematic characterization study is conducted to investigate the light-induced changes in the various a-Si:H nanostructures to understand the nature of the metastable defects.

First, all films on glass were characterized by DBPAS to identify the dominant type of open volume deficiency present in the nanostructure of the as-deposited state. The VEPFIT program was used to extract the Doppler S parameter of the films from the measured positron implantation depth profiles [43]. Since the positrons typically diffuse towards the open volumes after implantation, the S parameter is a measure for the size of the dominant open volume deficiency in a material, including semiconductors like a-Si:H [19,31,32,44–47]. We only report normalized $S/S_{c\text{-}Si}$ values to enable a comparison with literature values; a reference c-Si sample was measured for this purpose. Details of the DBPAS setup are described elsewhere [31,32]. These results are then compared with the total paramagnetic defect density, N_s, which is associated with the a-Si:H db density. This property was determined by double integration of the cw-EPR spectra following protocols described in the literature, which also describe further details of the setup [47,48]. Note that the cw-EPR experiments were performed using a Bruker ESP300 X-band spectrometer and a superhigh-quality Q-factor resonator operating at the TE_{011} microwave mode. cw-EPR measurements were carried out at a low microwave power of 0.2 mW to avoid signal saturation and an optimum lock-in modulation amplitude of 4 G was chosen. The values of $S/S_{c\text{-}Si}$ and N_s are plotted in Fig. 1(a) for all four a-Si:H samples both before and after light soaking. It is immediately clear that the porous $R = 0$ sample is dominated by nanosized voids, which corresponds to the high R^* value shown in Table I, while the other three materials are dominated by divacancies and can thus be considered dense. Generally, dense a-Si:H exhibits low N_s values while high N_s values indicate porous a-Si:H. Furthermore, N_s increases more strongly with $S/S_{c\text{-}Si}$ in the as-deposited state in comparison to the light-soaked state. Although the quality of the four films is different, the N_s values after light soaking are rather similar and N_s depends significantly on $S/S_{c\text{-}Si}$ only in the as-deposited state. This implies that there is a long-term defect creation process in the SWE which only weakly depends on the nanostructure. There was no measurable effect of LID on the Doppler parameters, so the $S/S_{c\text{-}Si}$ values before and after

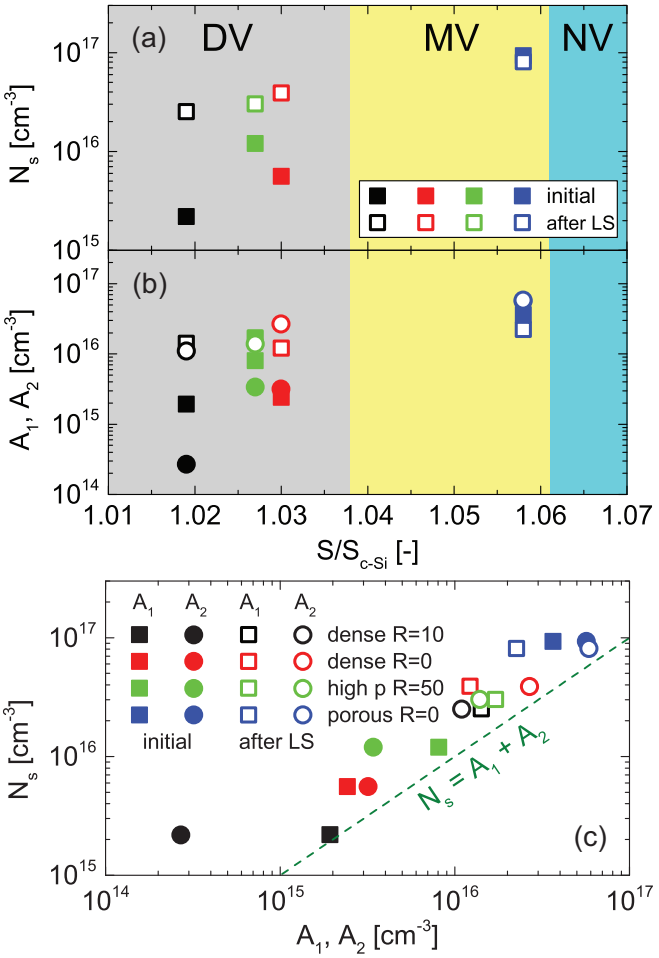

FIG. 1. (Color online) Dependence on (normalized) Doppler S parameter of (a) db density, N_s and (b) A_1 and A_2 for different a-Si:H materials both in the as-deposited state (initial) and light-soaked state (after LS), as well as (c) the relation between A_1 and A_2 and the db density. For different values of $S/S_{c\text{-}Si}$ the dominant type of open volume deficiency in the material can be either divacancies (DVs), multivacancies (MVs), or nanosized voids (NVs), as indicated by the colored areas [31].

light soaking are considered equal. This finding is explained by realizing that the size distribution of open volume deficiencies does not change significantly during LID.

Additional local information on the distribution of defect distances and the presence of defect clusters can be obtained from electron spin couplings. However, despite its power to identify paramagnetic centers and evaluate their quantity, field sweep cw-EPR spectroscopy typically does not provide the necessary spectral resolution to determine couplings between dilute electron spins in disordered materials such as a-Si:H. In this case, one has to resort to ESE techniques [49–52]. In particular, ESE decays are very sensitive to the coupling situation of db spins in a-Si:H [34]. Therefore, ESE decay measurements are used here to analyze the connection between the a-Si:H nanostructure and the light-induced changes in the material.

To extract this information, we performed ESE-detected phase memory time measurements employing a standard

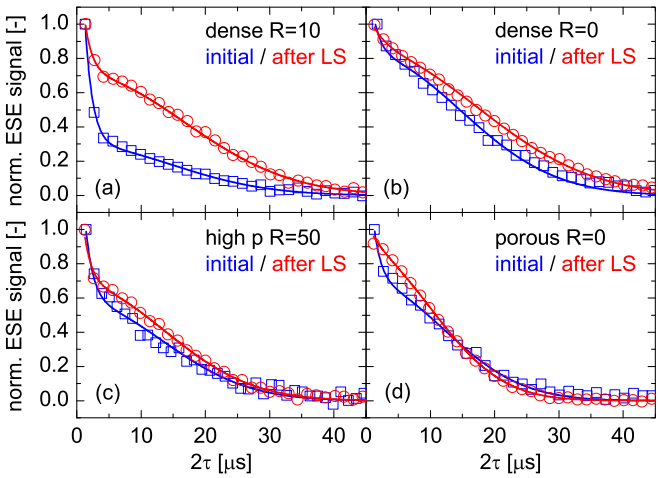

FIG. 2. (Color online) Normalized ESE decays of various a-Si:H materials (symbols) and fitted stretched-exponential functions (lines) both in the initial state (blue) and light-soaked state (red). All spectra were recorded at $g = 2.0055$.

two-pulse Hahn echo sequence ($\pi/2-\tau-\pi-\tau$–echo), with $\pi/2 = 44$ ns, $\pi = 88$ ns. For the detection of the ESE amplitude as a function of the pulse separation time, a starting value of $\tau = 640$ ns was chosen, which was then stepwise incremented by $\Delta\tau = 24$ ns. All relaxation decays were taken at the center of the db EPR spectrum ($g = 2.0055$). These pulsed X-band EPR experiments were performed at $T = 80$ K and a constant value of the magnetic field B_0 which was chosen to get a maximum ESE signal on a Bruker ElexSys E580 spectrometer equipped with a standard dielectric ring EPR resonator (Bruker ER3118X-MD5). The same samples were used for both the cw-EPR and ESE experiments.

To enable a direct comparison of the initial and light-soaked state for each sample, as well as a comparison between individual samples, we compare the normalized ESE decays, as shown in Fig. 2. For each sample we recorded ESE decays before and after light soaking. Obviously, differences in the local nanostructure surrounding a defect are detectable, as the echo decays are shaped differently for all four samples. It is particularly striking that the dense $R = 10$ material, which is the most stable material when used as an absorber layer in an a-Si:H solar cell, shows the largest difference in the ESE decay between the as-deposited and light-soaked state of all four samples considered. It is obvious that a simple monoexponential function can generally not describe all the ESE decays shown in Fig. 2. However, all the decays can be fitted extremely well when using the model of Fehr *et al.* [34] who describe the ESE signal V as a superposition of two exponentials:

$$V(2\tau) = A_1 \exp\left(\frac{-2\tau}{T_{SD,1}}\right) + A_2 \exp\left[-\left(\frac{\tau}{T_{SD,2}}\right)^2\right], \quad (1)$$

where A_1 and A_2 represent the amplitudes of individual EPR spectra while $T_{SD,1}$ and $T_{SD,2}$ are phase memory relaxation times associated with spectral diffusion (SD). The first monoexponential term in Eq. (1) corresponds to fast relaxing dbs (type 1) and was associated with interactions between

clustered electron spins. The second term in Eq. (1) originates from slowly decaying dbs (type 2) and was assigned to electron nuclear spin interactions of nonclustered spins [34]. Therefore, A_1 and A_2 represent the densities of type 1 and type 2 dbs, respectively. While fitting a minimum number of free variables in the fitting routine, we were able to maintain $T_{SD,1} = 1.2\ \mu s$ as a constant value for all fits shown in Fig. 2, while fitting yielded $T_{SD,2} = 9.6 \pm 1.3\ \mu s$ in the as-deposited state and $T_{SD,2} = 10.4 \pm 2.0\ \mu s$ in the light-soaked state. Our findings agree with the relaxation model proposed in [34], although we report somewhat lower $T_{SD,1}$ and $T_{SD,2}$ values in comparison to Fehr *et al.* ($T_{SD,1} = 2.4 \pm 1.0\ \mu s$; $T_{SD,2} = 11.4 \pm 1.0\ \mu s$). These differences may be due to differences in hydrogen concentration or other material peculiarities which are induced by a much higher deposition frequency (95 vs 13.56 MHz used in this work). Nevertheless, the ESE decays still need to be fitted with both a fast and a slowly relaxing component. This further supports the hypothesis that at least two types of defects are involved in the SWE [34].

After having obtained properly fitted ESE decays it can be assessed how much each of the two proposed defect types contributes to the db density. In Fig. 1(c), A_1 and A_2 are dependent on N_s, both before and after light soaking. Generally, A_1 and A_2 increase after light soaking, similar to the overall increase in N_s after light soaking as observed in Fig. 1(a). This is not surprising, since $N_s = A_1 + A_2$ as the modeled ensemble of type 1 and type 2 defects yield well-fitted ESE decays and together describe the total db density, but it can now be identified how much each of the two proposed defect types increases in density after light soaking. A closer inspection of Fig. 1(c) reveals that the relative increase of A_1 and A_2 varies substantially for the four different a-Si:H materials and thus depends on the nanostructure. However, based on EPR experiments alone it is difficult to infer the nature of the metastable defects present in the various a-Si:H materials.

A more direct and structural way to investigate the defects in a-Si:H is to combine our DBPAS findings with the ESE-EPR results. More specifically, the fitted ESE decays can be utilized to understand the nanostructural surroundings of the two proposed defect types when comparing A_1 and A_2 with the $S/S_{\text{c-Si}}$ values obtained from DBPAS, both before and after light soaking. The results of this analysis are depicted in Fig. 1(b). Using this visualization it is again clear that A_1 and A_2 both increase after light soaking. However, after light soaking, the moderate dependence of A_1 on $S/S_{\text{c-Si}}$ in the as-deposited state disappears completely, while the initially strong dependence of A_2 on $S/S_{\text{c-Si}}$ becomes only weak. Recently, A_1 and A_2 were suggested to be linked to defects in large open volume deficiencies and randomly distributed defects, respectively, but only based on EPR experiments [34].

However, with the extra nanostructural information that appears from combining our DBPAS and EPR results, we propose with more certainty which nanoscopic mechanisms are taking place during LID and assign a physical meaning to A_1 and A_2. A schematic sketch depicting the theoretically possible ways of creating dbs in small and large open volume deficiencies is shown in Fig. 3. Generally, a db can be formed when breaking Si-H bonds, which can occur at the surface of larger open volume deficiencies or in small open volume deficiencies. Depending on whether the formed unpaired spin is clustered or

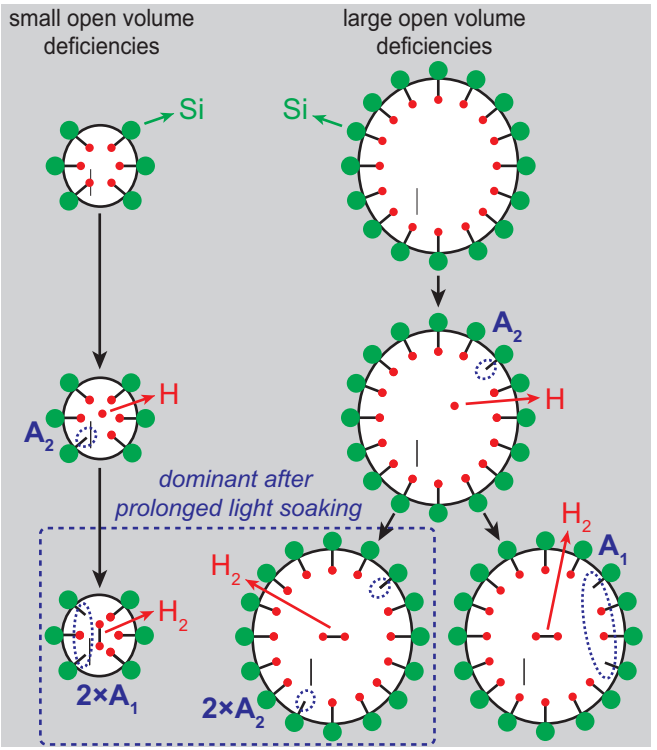

FIG. 3. (Color online) Schematic representation of a nanoscopic model of the LID in a-Si:H. The arrows indicate light-induced changes and the dashed blue ellipses indicate spin interaction, which is strongly distance dependent [34]. The dominant defect configurations in small and large open volume deficiencies after prolonged light soaking are marked in a blue rectangle. The gray area represents the material similar to a continuous random network in which the open volume deficiencies are embedded.

nonclustered, it will contribute to either A_1 or A_2, respectively, which can occur in both small and large open volume deficiencies. In the as-deposited state, A_1 increases moderately with $S/S_{\text{c-Si}}$ and A_2 increases strongly with $S/S_{\text{c-Si}}$. These dependencies indicate that the defects in the as-deposited state are mostly present in large open volume deficiencies, as the nanosized void density increases with increasing $S/S_{\text{c-Si}}$. Note that the defect configurations that contribute to A_1 and A_2 in large open volume deficiencies can be stable due to the presence of H_2 molecules which do not swiftly recombine with dbs to form Si-H bonds due to the relatively high H-H dissociation energy. After light soaking, the strong $A_2 - S/S_{\text{c-Si}}$ dependence weakens but is still clearly present, while A_1 is completely uncorrelated with $S/S_{\text{c-Si}}$. This implies that A_2 largely corresponds to light-induced defects created in large open volume deficiencies. Following this reasoning, A_1 could now be mostly linked to light-induced defects in isotropically distributed small open volume deficiencies or linked to isotropically distributed defects present in the matrix which surrounds the open volume deficiencies and which is similar to a continuous random network. However, the amount of such material similar to a continuous random network should decrease when the nanosized void density increases and since A_1 and $S/S_{\text{c-Si}}$

are uncorrelated after light soaking, A_1 likely corresponds to defects that are predominantly present in small open volume deficiencies.

Considering all of the above, we propose that reducing the nanosized void density while increasing the H passivation degree of small open volume deficiencies as much as possible—for instance, by depositing at $R > 0$ and/or using a triode reactor [19]—is the recipe for making the most stable a-Si:H. Such an enhanced understanding of the formation of light-induced defects is an important step forward in comprehending the nature of metastable defects in a-Si:H and reducing the SWE. Solving this 38-year-old problem would lead to significant improvements in the production process of a-Si:H based solar cells, but is also relevant for other production processes that include a-Si:H, such as silicon heterojunction solar cells [53], optical sensors and thin-film transistors [54], and, more recently, waveguides for telecommunication applications such as photonic chips and optical fibers [55].

We gratefully acknowledge Sebastian Neubert from PVcomB for his assistance in the light soaking experiments. Further, we acknowledge financial support for this research from ADEM, A green Deal in Energy Materials of the Ministry of Economic Affairs of The Netherlands (www.adem-innovationlab.nl) and the STW Vidi project of one of the authors (A.H.M.S.) from Delft University of Technology, Grant No. 10782. This work has been supported by the European Union [FP7/2007-2013] under Grant Agreement No. 262533 (SOPHIA), project ANSSAL, and the Deutsche Forschungsgemeinschaft (DFG) within priority program SPP 1601.

[1] D. L. Staebler and C. R. Wronski, Appl. Phys. Lett. **31**, 292 (1977).
[2] D. L. Staebler and C. R. Wronski, J. Appl. Phys. **51**, 3262 (1980).
[3] M. Stutzmann, W. B. Jackson, and C. C. Tsai, Phys. Rev. B **32**, 23 (1985).
[4] S. T. Pantelides, Phys. Rev. Lett. **57**, 2979 (1986).
[5] S. T. Pantelides, Phys. Rev. B **36**, 3479 (1987).
[6] W. B. Jackson, Phys. Rev. B **41**, 10257 (1990).
[7] S. B. Zhang, W. B. Jackson, and D. J. Chadi, Phys. Rev. Lett. **65**, 2575 (1990).
[8] H. M. Branz, Phys. Rev. B **59**, 5498 (1999).
[9] H. Fritzsche, Annu. Rev. Mater. Res. **31**, 47 (2001), and references therein.
[10] C. Longeaud, D. Roy, and O. Saadane, Phys. Rev. B **65**, 085206 (2002).
[11] M. J. Powell, S. C. Deane, and R. B. Wehrspohn, Phys. Rev. B **66**, 155212 (2002).
[12] P. Stradins, Sol. Energy Mater. Sol. Cells **78**, 349 (2003).
[13] T. Shimizu, Jpn. J. Appl. Phys. **43**, 3257 (2004), and references therein.
[14] J. Melskens, G. van Elzakker, Y. Li, and M. Zeman, Thin Solid Films **516**, 6877 (2008).
[15] A. H. M. Smets, C. R. Wronski, M. Zeman, and M. C. M. van de Sanden, Mater. Res. Soc. Symp. Proc. **1245**, A-14-02 (2010).
[16] M. Stuckelberger, M. Despeisse, G. Bugnon, J.-W. Schüttauf, F.-J. Haug, and C. Ballif, J. Appl. Phys. **114**, 154509 (2013).
[17] C. R. Wronski and X. Niu, IEEE J. Photovoltaics **4**, 778 (2014).
[18] J. Melskens, M. Schouten, R. Santbergen, M. Fischer, R. Vasudevan, D. J. van der Vlies, R. J. V. Quax, S. G. M. Heirman, K. Jäger, V. Demontis, M. Zeman, and A. H. M. Smets, Sol. Energy Mater. Sol. Cells **129**, 70 (2014)
[19] J. Melskens, M. Schouten, A. Mannheim, A. S. Vullers, Y. Mohammadian, S. W. H. Eijt, H. Schut, T. Matsui, M. Zeman, and A. H. M. Smets, IEEE J. Photovoltaics **4**, 1331 (2014).
[20] M. Stuckelberger, Y. Riesen, M. Despeisse, J.-W. Schüttauf, F.-J. Haug, and C. Ballif, J. Appl. Phys. **116**, 094503 (2014).
[21] M. Stuckelberger, A. Billet, Y. Riesen, M. Boccard, M. Despeisse, J.-W. Schüttauf, F.-J. Haug, and C. Ballif, Prog. Photovoltaics Res. Appl. (2014).
[22] B. Yan, G. Yue, L. Sivec, J. Yang, S. Guha, and C.-S. Jiang, Appl. Phys. Lett. **99**, 113512 (2011).
[23] G. Yue, B. Yan, L. Sivec, T. Su, Y. Zhou, J. Yang, and S. Guha, Mater. Res. Soc. Symp. Proc. **1426**, 33 (2012).
[24] S. Kim, J.-W. Chung, H. Lee, J. Park, Y. Heo, and H.-M. Lee, Sol. Energy Mater. Sol. Cells **119**, 26 (2013).
[25] L. Yang and L. F. Chen, Mater. Res. Soc. Symp. Proc. **336**, 669 (1994).
[26] J. Yang, X. Xu, and S. Guha, Mater. Res. Soc. Symp. Proc. **336**, 687 (1994).
[27] A. Matsuda, T. Kaga, H. Tanaka, and K. Tanaka, J. Non-Cryst. Solids **59-60**, 687 (1983).
[28] T. Matsui, H. Sai, K. Saito, and M. Kondo, Prog. Photovoltaics Res. Appl. **21**, 1363 (2013).
[29] W. M. M. Kessels, A. H. M. Smets, D. C. Marra, E. S. Aydil, D. C. Schram, and M. C. M. van de Sanden, Thin Solid Films **383**, 154 (2001).
[30] D. E. Polk, J. Non-Cryst. Solids **5**, 365 (1971).
[31] J. Melskens, A. H. M. Smets, S. W. H. Eijt, H. Schut, E. Brück, and M. Zeman, J. Non-Cryst. Solids **358**, 2015 (2012).
[32] J. Melskens, A. H. M. Smets, M. Schouten, S. W. H. Eijt, H. Schut, and M. Zeman, IEEE J. Photovoltaics **3**, 65 (2013).
[33] M. Fehr, A. Schnegg, B. Rech, K. Lips, O. Astakhov, F. Finger, G. Pfanner, C. Freysoldt, J. Neugebauer, R. Bittl, and C. Teutloff, Phys. Rev. B **84**, 245203 (2011).
[34] M. Fehr, A. Schnegg, B. Rech, O. Astakhov, F. Finger, R. Bittl, C. Teutloff, and K. Lips, Phys. Rev. Lett. **112**, 066403 (2014).
[35] A. H. M. Smets, W. M. M. Kessels, and M. C. M. van de Sanden, Appl. Phys. Lett. **82**, 1547 (2003).
[36] A. H. M. Smets and M. C. M. van de Sanden, Phys. Rev. B **76**, 073202 (2007).
[37] E. Bhattacharya and A. H. Mahan, Appl. Phys. Lett. **52**, 1587 (1988).
[38] M. Fischer, R. J. V. Quax, M. Zeman, and A. H. M. Smets, in *39th IEEE Photovoltaic Specialists Conference Proceedings, Tampa, FL* (IEEE, Piscataway, 2013).
[39] H. Tan, E. Psomadaki, O. Isabella, M. Fischer, P. Babal, R. Vasudevan, M. Zeman, and A. H. M. Smets, Appl. Phys. Lett. **103**, 173905 (2013).
[40] H. Tan, P. Babal, M. Zeman, and A. H. M. Smets, Sol. Energy Mater. Sol. Cells **132**, 597 (2014).

[41] M. Fischer, H. Tan, J. Melskens, R. Vasudevan, M. Zeman, and A. H. M. Smets, Appl. Phys. Lett. **106**, 043905 (2015).
[42] J.-H. Zhou, M. Kumeda, and T. Shimizu, Phys. Rev. B **53**, 7267 (1996).
[43] A. van Veen, H. Schut, J. de Vries, R. A. Hakvoort, and M. R. IJpma, AIP Conf. Proc. **218**, 171 (1991).
[44] X. Zou, Y. C. Chan, D. P. Webb, Y. W. Lam, Y. F. Hu, C. D. Beling, S. Fung, and H. M. Weng, Phys. Rev. Lett. **84**, 769 (2000).
[45] P. M. Gordo, M. F. Ferreira Marques, C. Lopes Gil, A. P. de Lima, G. Lavareda, C. Nunes de Carvalho, A. Amaral, and Zs. Kajcsos, Radiat. Phys. Chem. **76**, 220 (2007).
[46] P. J. Schultz and K. G. Lynn, Rev. Mod. Phys. **60**, 701 (1988).
[47] F. Tuomisto and I. Makkonen, Rev. Mod. Phys. **85**, 1583 (2013).
[48] M. Fehr, P. Simon, T. Sontheimer, C. Leendertz, B. Gorka, A. Schnegg, B. Rech, and K. Lips, Appl. Phys. Lett. **101**, 123904 (2012).
[49] J. R. Klauder and P. W. Anderson, Phys. Rev. **125**, 912 (1962).
[50] W. B. Mims, Phys. Rev. **168**, 370 (1968).
[51] P. Hu and S. R. Hartmann, Phys. Rev. B **9**, 1 (1974).
[52] K. M. Salikhov, S. A. Dzuba, and A. M. Raitsimring, J. Magn. Reson. **42**, 255 (1981).
[53] A. Descoeudres, Z. C. Holman, L. Barraud, S. Morel, S. de Wolf, and C. Ballif, IEEE J. Photovoltaics **3**, 83 (2013).
[54] *Technology and Applications of Amorphous Silicon*, edited by R. A. Street (Springer-Verlag, Germany, 2000).
[55] F. Leo, J. Safioui, B. Kuyken, G. Roelkens, and S.-P. Gorza, Opt. Express **22**, 28997 (2014).